Journal of Alloys and Compounds 480 (2009) 295–298

Contents lists available at ScienceDirect

Journal of Alloys and Compounds

journal homepage: www.elsevier.com/locate/jallcom

Effect of melt convection on the secondary dendritic arm spacing in peritectic Nd–Fe–B alloy

K. Biswas[a,*], R. Hermann[a], H. Wendrock[a], J. Priede[b,c], G. Gerbeth[b], B. Buechner[a]

[a] Leibniz Institute for Solid State and Materials Research (IFW) Dresden, P.O. Box 270116, D-01171 Dresden, Germany
[b] Forschungszentrum Rossendorf (FZR), Institute of Safety Research, P.O. Box 510119, 01314 Dresden, Germany
[c] Applied Mathematics Research Centre, Department of Mathematical Sciences, Coventry University, Priory Street, Coventry CV1 5FB, UK

ARTICLE INFO

Article history:
Received 9 November 2008
Received in revised form 16 January 2009
Accepted 24 January 2009
Available online 6 February 2009

Keywords:
Peritectic solidification
Nd–Fe–B
Secondary dendritic arm spacing
Melt-convection

ABSTRACT

Dendrites are one of the major microstructural constituents of peritectic alloys. In the present work, the effect of melt convection on the secondary dendritic arm spacing (SDAS) and volume fraction of properitectic α-Fe was investigated during solidification of stoichiometric Nd–Fe–B alloys using the forced crucible rotation technique. The resulting microstructure of the alloy in consideration of melt convection has been investigated using scanning electron microscopy and optical microscopy. The average SDAS was determined for each sample from the whole cross-section of the cylindrical test samples using image analyzing software LEICA QWIN. A detailed statistical analysis of the spacing distribution was performed on the basis of the variation of SDAS values, averaged from about 80 to 120 dendrites in different zones. The α-Fe volume fraction, measured by vibrating sample magnetometer (VSM), reduces with increasing crucible rotation frequency. Similarly, the SDAS values decrease with increasing rotation frequency. These results are explained from the viewpoint of a reduced melt convection state under steady forced crucible rotation leading to a reduced effective mass transfer coefficient.

1. Introduction

Peritectic solidification has drawn huge attention in both experimental and theoretical studies due to the wide application field of many peritectic alloys [1,2]. Extensive investigations have been done to understand the solidification behaviour of the properitectic phase, the morphology of properitectic phase, and the evolved microstructures for different peritectic alloys. Especially, Ti–Al-based alloys and Nd–Fe–B-based rare earth permanent magnets exhibit attractive properties like high strength at high temperatures and excellent hard magnetic properties, respectively [1–3]. The change in volume fraction and morphology of the properitectic phase is the topic of prime importance as these microstructural parameters play an important role in determining the magnetic and mechanical properties of Nd–Fe–B [4] and Ti–Al alloys, respectively [5]. However, there is still a lack of understanding of the transformation mechanisms and the influences of many aspects such as melt convection during peritectic solidification which plays an important role concerning magnetic and mechanical properties [6–7].

The dendritic structure, which is commonly observed in peritectic microstructure, is a key microstructural feature and is characterized by the primary and secondary dendritic arm spacing (SDAS). Numerous studies have been done during the last years to investigate the effect of convection during directional solidification experiments on the primary and secondary dendritic arm spacings of several alloys like Sn–Pb, Al–Cu, Pb–Sb systems [8–10]. But little is known about the influence of natural or forced convection on the microstructure development of peritectic alloys. There is no report on the effect of melt convection on the SDAS of properitectic phase of any alloy during conventional solidification process.

In comparison with the amount of work done on the measurement of SDAS as a function of cooling rate, there is relatively little information on the effect of other solidification parameters like effective mass transfer coefficient and fluid flow velocity on SDAS. Solidification studies have been reported with a view to characterize primary dendrite arm spacing (λ_1), secondary dendrite arm spacing (λ_2) and dendrite tip radius (R) as a function of initial alloy solute concentration (C_0), growth rate (V) and temperature gradient (G) ahead of the microscopic solidification front together with extensive theoretical studies [11,12] and models [13–19]. Langer and Müller-Krumbhaar [14] have carried out a detailed numerical analysis of the wavelength of instabilities along the sides of a dendrite.

* Corresponding author. Current address: Glass Technology Laboratory, Central Glass and Ceramic Research Institute, 196, Raja S.C. Mullick Road, Kolkata 32, India. Tel.: +91 9748051040; fax: +91 33 2473 0957.
E-mail address: kk.biswas@gmail.com (K. Biswas).

0925-8388/$ – see front matter © 2009 Published by Elsevier B.V.
doi:10.1016/j.jallcom.2009.01.106

Kattamis and Flemings [20] and Feurer and Wunderlin [21] showed that the secondary dendrite arm spacing (λ_2) is dependent on solidification time (t_f).

Beckermann et al. [22] and Diepers et al. [23] introduced models concerning the effect of flow condition on the coarsening rate of secondary arms for Al–4 wt.%Cu alloy. Diepers et al. calculated the coarsening rate of secondary arms on two different bases, the time evolution of the mean radius of curvature and the time evolution of the specific surface area.

Fredriksson et al. [24] found that fluid flow increases dendrite spacing within the equiaxed zone for Al-based alloys. Recently, Steinbach et al. [25] studied the effect of rotating magnetic field on the microstructure formation during the directional solidification of Al–Si–Mg alloy and showed that with increasing fluid flow, SDAS increases.

Ma et al. [26] showed that the arm coarsening of primary properitectic dendrites is influenced by the peritectic reaction, as the secondary peritectic phase provides an additional solute diffusion flux due to the phase transformation.

Recent studies by Hermann et al. [27] on Nd–Fe–B alloys with forced rotation experiments and global crucible rotation revealed a decrease of the volume fraction of properitectic α-Fe dendrites with increasing rotational frequency. Numerical simulation by Shatrov et al. [28] showed that fast rotation suppresses the internal flow considerably in levitated droplets during electromagnetic levitation.

In this article, the effect of reduced melt convection on the SDAS of the properitectic α-Fe phase was investigated for stoichiometric Nd–Fe–B alloy. A systematic study was performed to determine the average SDAS of α-Fe dendrites in samples solidified at different rotational frequencies. The variation of SDAS values is explained in terms of convection states.

2. Experimental

A master alloy of $Nd_{11.8}Fe_{82.3}B_{5.9}$ was prepared from pure Fe (99.9%, Alfa Aesar), Nd (99.99%, Goodfellow) and FeB powder (99%, Mateck GmbH) and cast to rods (6 mm diameter) using a cold crucible levitation melting facility.

For the forced rotation experiments, the samples were sealed in quartz ampoules at Ar pressure of 500 mbar. The ampoules could not be filled up to normal atmospheric Ar pressure because of the strong gas expansion at high temperature. The ampoules were prepared from commercially available quartz tubes with inner diameter of 10 mm and wall width of 1.5 mm. The top part of the ampoules was specially designed so that it can be attached to the quartz tube at two grooves on the top. This quartz tube is mechanically connected to an AC motor, which can be operated at variable frequencies (0–2500 rpm) as shown in Fig. 1. An induction coil is wrapped around the quartz tube and connected to a high frequency power supply (100 kHz, 50 kW). Samples were heated up to 1350 °C by induction heating. When the sample is completely molten, the AC motor is switched on, enabling the ampoule to rotate at a defined rotational frequency. The quartz ampoule with the molten metal is rotated for 90 s. The solidification of the metal was initiated by switching off the power supply of the generator. The cooling rate measured with a two-color pyrometer was approximately 40 K/s for both rotating (at 1200 rpm) and non-rotating cases. The solidified cylindrical samples were cut into two pieces along the vertical symmetry axis of the cylindrical mass by using an electroerosive cutting machine (Seibu-50). One half was used for the determination of the α-Fe volume fraction by VSM and the second half for scanning electron microscopy investigations (SEM).

For VSM measurements, the half cylindrical mass was broken into small pieces. To minimize oxidation during heating, a single piece of about 45–50 mg was taken for each measurement. The piece was closed in Ag foil and fixed in a BN crucible. Measurements were done in protective Ar atmosphere. The VSM measurements were carried out in a magnetic field of 1.8 T at a temperature of 350 °C. The temperature (350 °C) was chosen above the Curie temperature of $Nd_2Fe_{14}B$ phase (312 °C), in order to measure the magnetization moment only from the ferromagnetic α-Fe phase. The effect of the paramagnetic matrix was eliminated considering the slope of the magnetization curves at fields higher than 1 T. Additionally, the magnetization of pure iron was measured at 350 °C for calibration. The α-Fe volume fraction of a sample was determined within an error limit of 0.3 wt.%.

For the determination of the SDAS, the samples were etched with 2% Nital (2 ml nitric acid in 98 ml ethanol) for 5 s before investigating with optical microscopy.

The used optical microscope was equipped with a motorized stage. A program was created as a Macro sequence (QUIPS routine) for the image analyzing system QTM 550/QWIN (LEICA Co.), which enables to inspect a large sample area field-by-field.

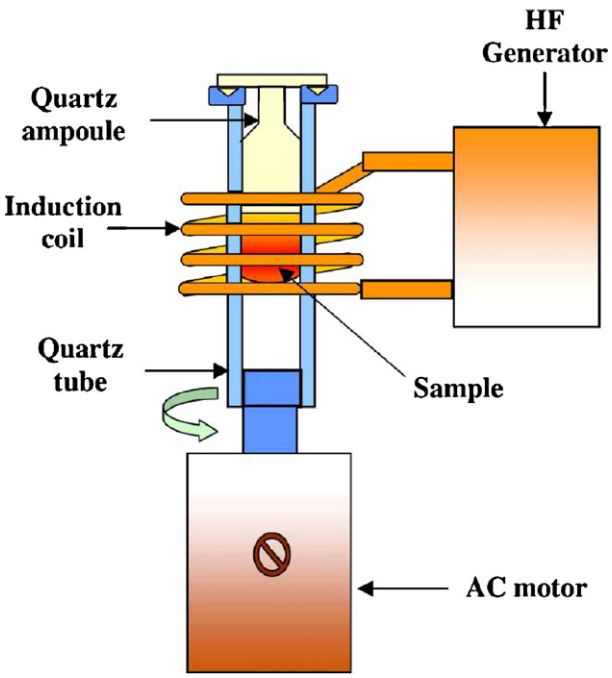

Fig. 1. Schematic diagram of forced rotation facility.

The measurement starts with an initialization segment where different parameters like the magnification, size of inspection area, total number of fields, the area of each field, and the overlap of neighboring fields are defined, and then a field-by-field imaging followed by interactive registration of all dendrite sections which are suitable for evaluation is realized. The field of inspection steps along the cross-section in a meander-like path and an image of sample are displayed at the screen for interactive acquisition of the dendrites. Only dendrites with clearly visible primary dendrite "stems" are recorded to ensure that they are sectioned parallel to their axis within a small angle uncertainty. The acquisition includes two steps:

- Mark a primary dendrite segment of length L by a vector line along its axis.
- Draw in the crossing point of each secondary dendrite arm with the primary dendrite along the segment L.

As illustrated in Fig. 2, the number of points (N) where primary and secondary dendritic arms intersect each other is counted automatically by the software and the mean secondary dendritic arm spacing λ_2 is calculated as,

$$\lambda_2 = \frac{L}{N-1}, \quad (1)$$

In this procedure, image files of each field and data (e.g. field number, coordinates of dendrite, length of primary segment and number of secondary arms) of each

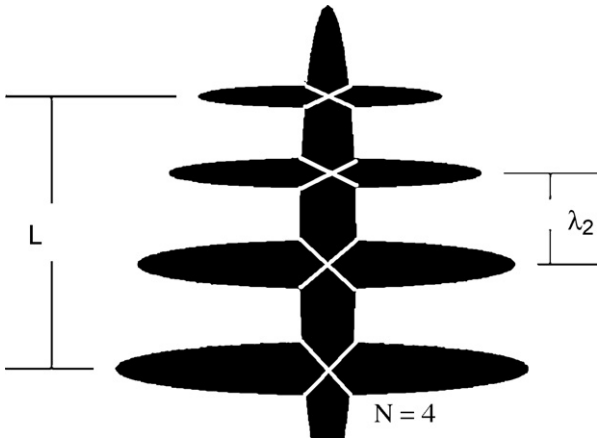

Fig. 2. Schematic representation of the method used for measurement of secondary dendritic arm spacing. The points indicated with cross are the number of secondary arms (N).

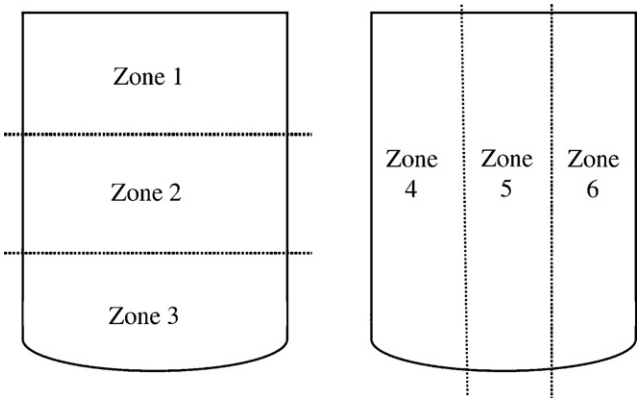

Fig. 3. Schematic representation of the six different zones for SDAS measurement.

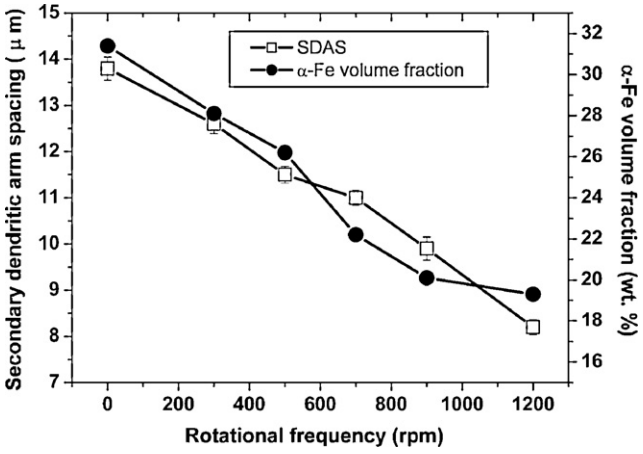

Fig. 4. The SDAS values and the α-Fe volume fraction vs. rotational frequency.

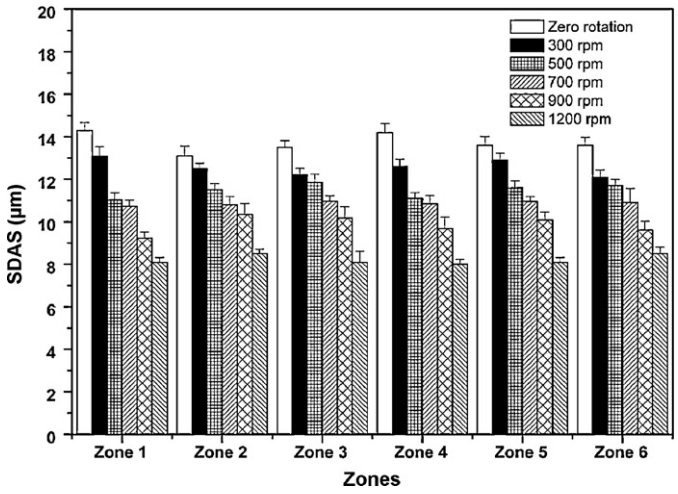

Fig. 5. The variation of SDAS values with standard error in the selected zones along the cross-section at various rotational frequency (0–1200 rpm).

selected dendrite are stored and a statistical data set is finally generated. The SDAS value is averaged from around 80 to 100 dendrites for each sample. The variation of SDAS values for different samples is obtained in the different zones along the cross-section as shown in Fig. 3.

3. Results and discussions

Fig. 4 shows the variation of SDAS and the α-Fe volume fraction in dependence on the rotational frequency (from 0 up to 1200 rpm). A drastic reduction of the α-Fe volume fraction and the SDAS of α-Fe dendrites is observed with increasing rotational frequency. Fig. 5 shows the variation of SDAS values with standard error in the selected six zones (see Fig. 3).

No significant variation in the SDAS values was observed in the different zones at a particular rotational frequency. This indicates a

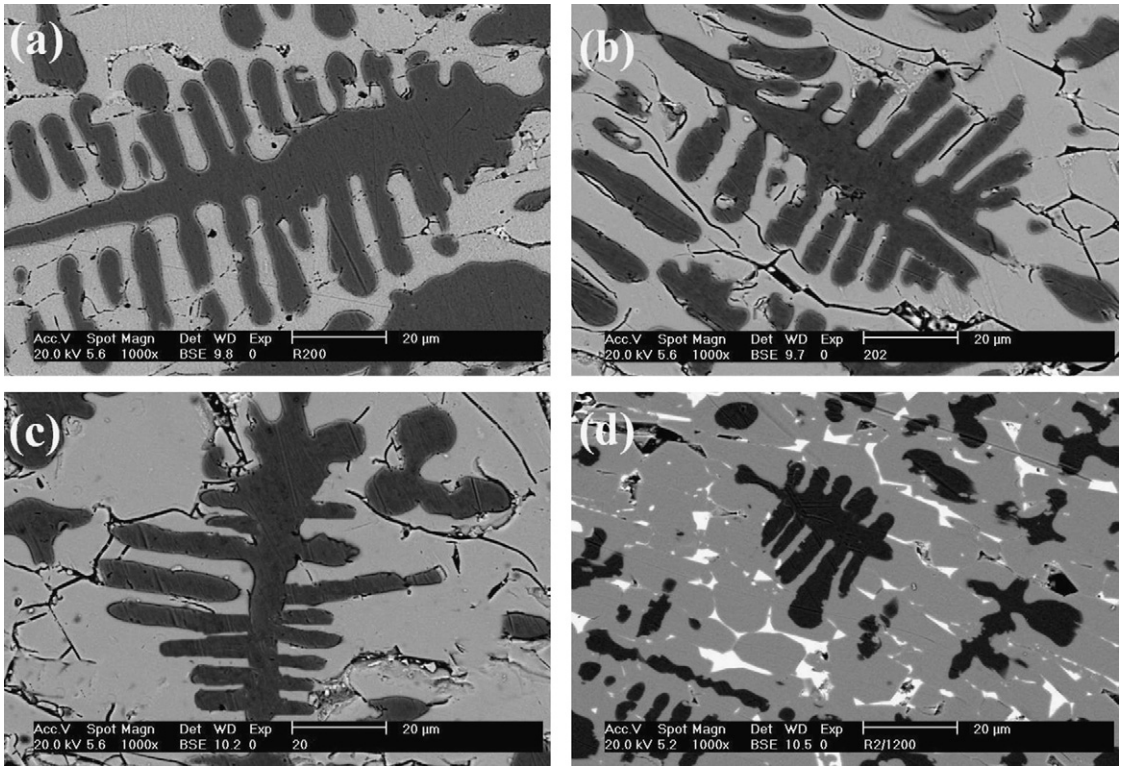

Fig. 6. SEM micrographs of samples solidified under 500 mbar Ar pressure at (a) 0 rpm, (b) 500 rpm, (c) 700 rpm and (d) 1200 rpm showing representative dendrites.

homogeneous distribution of the SDAS in the microstructure over the full cross-section suggesting that the effective mass transfer does not vary significantly along the length or width of the investigated melt volume.

Fig. 6 represents the SEM micrographs of samples solidified at zero, 500, 700 and 1200 rpm showing the morphology of α-Fe dendrites with secondary dendritic arms. The decrease of SDAS is clearly visible from Fig. 6(a)–(d) as the rotational frequency increases. As discussed earlier, the melt convection decreases when increasing the rotational frequency. Thus, both the volume fraction and SDAS of α-Fe dendrites decrease in a reduced melt convection state. The secondary dendrite arms are coarsened in the samples solidified under strong convection (as shown in Fig. 6(a)) compared to samples solidified under reduced convection state (as shown in Fig. 6(d)).

As the measured cooling rate for both the rotating (1200 rpm) and non-rotating cases are quite similar (40 K/s), the influence of cooling rate on the reduction of the phase fraction and SDAS of properitectic phase can be neglected. Thus it can be inferred that the microstructural change is mainly caused by the different convection states. The formation mechanism of the refined morphology of dendrites under reduced melt convection is not well understood. We attribute the reduction in the phase fraction and SDAS of properitectic phase to the reduced convective mass transfer under reduced internal melt motion.

The mass transfer includes both convection and diffusion. Mass transfer coefficients can be estimated from different theoretical equations, correlations, and analogies that are functions of material properties and flow regimes (laminar or turbulent flow). Selection of the most applicable model is dependent on the materials and the system, or environment, being studied.

With high fluid velocity, the enhanced interdendritic flow reduces the solute boundary layer and increases the transfer of solute from the interface, removing the barrier to the growth of dendrites. Additionally, under strong convection, smaller arms dissolve into the melt making the SDAS higher.

The findings of Fredriksson et al. [24] and Steinbach et al. [25] corroborate our results obtained from forced rotation experiments for peritectic Nd–Fe–B alloy as they also reported for Al-based alloys that under strong stirring, SDAS increases.

The presence of soft magnetic α-Fe together with hard magnetic $Nd_2Fe_{14}B$ is detrimental for the superior hard magnetic properties of Nd–Fe–B-based magnets. Properitectic α-Fe volume fraction can be lowered by using this novel forced rotation facility. This reduction of properitectic soft magnetic α-Fe volume fraction is beneficial for ingot preparation by induction melting.

4. Summary

The effect of melt convection on the solidification process and the microstructure evolution of Nd–Fe–B alloys were investigated experimentally with a specially designed forced crucible rotation technique. Numerical simulations of the fluid flow suggested that a global melt rotation suppresses the internal melt motion significantly compared to the non-rotating case. The experiments with different rotational frequencies resulted in a strong reduction of both the soft magnetic α-Fe phase volume fraction and the SDAS at increased global crucible rotation corresponding to reduced internal melt motion. The SDAS value for the investigated stoichiometric Nd–Fe–B alloy is 13.8 μm at zero rotational frequency, whereas it decreases to 8.2 μm for the sample solidified at 1200 rpm. The measured cooling rates for both the cases were similar (40 K/s) and thus, it was concluded that the microstructural difference is caused by the variation of convection states. The stronger interdendritic flow at high fluid velocity and at low rotational frequency reduces the solute boundary layer and increases the transfer of solute from the interface. Under strong convection, smaller dendrite arms dissolve into the melt and solute is transported to make the SDAS higher.

Acknowledgements

Financial support provided by Deutsche Forschungsgemeinschaft within the framework of Priority program 1120 “Phase Transformation in Multicomponent Melts” (HE2955/2-2) and Sonderforschungsbereich 609 “Elektromagnetische Strömungsbeeinflussung in Metallurgie, Kristallzüchtung und Elektrochemie” is gratefully acknowledged. One of the authors (K. Biswas) is grateful to Dr H.S. Maiti, Director, CGCRI, Calcutta, for his permission to publish this paper.

References

[1] H.W. Kerr, W. Kurz, Int. Mater. Rev. 41 (1996) 129–164.
[2] M. Sagawa, S. Fujimura, N. Togawa, H. Yamamoto, Y. Matsuura, J. Appl. Phys. 55 (1984) 2083–2087.
[3] W.J. Boettinger, S.R. Coriell, A.L. Greer, A. Karma, W. Kurz, M. Rappaz, R. Trivedi, Acta Mater. 48 (2000) 43–70.
[4] T. Umeda, T. Okane, W. Kurz, Acta Mater. 44 (1996) 4209–4216.
[5] D. Ma, Y. Li, S.C. Ng, H. Jones, Acta Mater. 48 (2000) 1741–1751.
[6] M.E. Glicksman, M.B. Koss, Phys. Rev. Lett. 73 (1994) 573–576.
[7] R. Trivedi, W. Kurz, Inter. Mater. Rev. 39 (1994) 49–74.
[8] M.D. Dupouy, D. Camel, J.J. Favier, Acta Metall. 37 (1989) 1143–1157.
[9] M. Li, T. Mori, H. Iwasaki, Mater. Sci. Eng. A 265 (1999) 217–223.
[10] H. Chen, Y.S. Chen, X. Wu, S.N. Tewari, J. Cryst. Growth 253 (2003) 413–423.
[11] S.Z. Lu, J.D. Hunt, J. Cryst. Growth 123 (1992) 17–34.
[12] J.D. Hunt, Acta Metall. Mater. 38 (1990) 411–418.
[13] J.D. Hunt, S.Z. Lu, Metall. Mater. Trans. A 27 (1996) 611–623.
[14] J.S. Langer, H. Müller-Krumbhaar, Acta Metall. 26 (1978) 1681–1687.
[15] V. Laxman, Acta Metall. 33 (1985) 1037–1049.
[16] W. Kurz, D.J. Fisher, Acta Metall. 29 (1981) 11–20.
[17] R. Trivedi, Metall. Mater. Trans. A 15 (1984) 977–982.
[18] D. Bouchard, J.S. Kirkaldy, Metall. Mater. Trans. B 27 (1996) 101–113.
[19] R. Trivedi, K. Somboonsuk, Mater. Sci. Eng. A 65 (1984) 65–74.
[20] T.Z. Kattamis, M.C. Flemings, Trans. Metall. Soc. AIME 233 (1965) 992–999.
[21] U. Feurer, R. Wunderlin, in: W. Kurz, D.J. Fisher (Eds.), Fundamentals of Solidification, Appendix 8, Trans. Tech. Publications Ltd., Aedermannsdorf, Switzerland, 1989, pp. 214–216.
[22] C. Beckermann, H.-J. Diepers, I. Steinbach, A. Karma, X. Tong, J. Comp. Phys. 154 (1999) 468–496.
[23] H.-J. Diepers, C. Beckermann, I. Steinbach, Acta Mater. 47 (1999) 3663–3678.
[24] H. Fredriksson, El. N. Mahallawy, M. Taha, L. Xiang, G. Wänglöw, Scand. J. Metall. 15 (1986) 127–137.
[25] S. Steinbach, L. Ratke, Mater. Sci. Eng. A 413–414 (2005) 200–204.
[26] D. Ma, W. Xu, S.C. Ng, Y. Li, Mater. Sci. Eng. A 390 (2005) 52–62.
[27] R. Hermann, O. Filip, G. Gerbeth, J. Priede, L. Schultz, J. Magn. Magn. Mater. 272 (2004) 1855–1856.
[28] V. Shatrov, J. Priede, G. Gerbeth, Phys. Fluids 19 (2007) 078106.